Title: Strong piezoelectric properties and electric-field-driven changes in domain structures in a PbZr0.87Ti0.13O3 single crystal

Author: Iwona Lazar, Andrzej Majchrowski, Dariusz Kajewski, Andrzej Soszyński, Krystian Roleder

UNIWERSYTET ŚLĄSKI W KATOWICACH

Biblioteka Uniwersytetu Śląskiego

Ministerstwo Nauki i Szkolnictwa Wyższego

Strong piezoelectric properties and electric-field-driven changes in domain structures in a $PbZr_{0.87}Ti_{0.13}O_3$ single crystal

Iwona Lazar [a,*], Andrzej Majchrowski [b], Dariusz Kajewski [a], Andrzej Soszyński [a], Krystian Roleder [a]

[a] *Institute of Physics, University of Silesia ul. 75 Pułku Piechoty 1, 41-500 Chorzów, Poland*
[b] *Institute of Applied Physics, Military University of Technology ul. Kaliskiego 2, 00-908 Warsaw, Poland*

ARTICLE INFO

ABSTRACT

$PbZr_{1-x}Ti_xO_3$ perovskite materials, known as PZT, are highly applicable, mainly due to their extraordinary piezoelectric properties. Recently, a technology of PZT crystals growth has been elaborated and opened new investigation possibilities for these compounds. In this paper, we demonstrate a highly piezoelectric response in $PbZr_{0.87}Ti_{0.13}O_3$ single crystal. Under the action of an electric field, the piezoelectric coefficient d_{33} turns out to be over 2500 pm V^{-1}. The optical studies performed have proved a significant influence of the domain dynamics on such high-efficiency piezoelectric response. Monoclinic M and rhombohedral R phases have been observed in the lead zirconate-titanate crystals with a low Ti content. This coexistence of phases with different symmetries and dense domain walls are the primary sources of high piezoelectric response. We have observed that strong electric fields may act on randomly oriented polarization vectors so that the total piezoelectric activity disappears, and the unusual isotropization point near 250 °C appears.

1. Introduction

Piezoelectric materials, classified as smart materials, are widely used in electronics [1,2], medical imaging, biomaterials medicine [3], sports [4], piezoelectric clothing [5], as well as in automotive industry [6] or in research devices e.g. high precision positioning systems [1,7]. Moreover, alternative energy sources are currently developed and, due to the fact that piezoelectric elements convert mechanical energy (pressure or vibration) into electricity, much research has been focused on how to use them as piezoelectric energy harvesting systems [8,9]. Despite numerous applications, systems with the highest piezoelectric coefficients are still sought for. Currently, the most effective and commonly used materials are those with a perovskite structure. To determine the origin of high-efficiency piezoelectric properties, numerous research projects have already been conducted. The proposed polarization rotation model [10-13] describes how the spontaneous polarization vector rotates and in consequence produces high piezoelectricity. Such an explanation has been used in single-crystal materials, such as $PbZr_{1-x}Ti_xO_3$ (abbreviated as PZT), $Pb(Zn_{1/3}Nb_{2/3})O_3–PbTiO_3$ (PZN–PT), and $Pb(Mg_{1/3}Nb_{2/3})O_3–PbTiO_3$ (PMN–PT), which revealed much stronger piezoelectric properties than analogous ceramics. It is believed that the appearance of monoclinic deformation of the perovskite unit cell is necessary for the high level of piezoelectric response induced by the rotation of polarization under electric field [11,14,15]. Due to the difficulties concerning the growth of the PZT crystals, the experimental verification of the theoretical rotation of polarization in such system is still needed. Especially because, according to the diagram by Zhang [16], the structures of PZT solid solutions are complex, and local monoclinic phases exist for all Ti content levels in the range of $0.08 < x < 0.5$.

Piezoelectric PZT solid solutions belong to the most known ones. They are oxidic perovskites for which the phase diagram (for ceramics) was first established by Jaffe [17]. At room temperature, PZT becomes piezoelectric above the Ti concentration of $x = 0.08$ [16,17], and at about $x = 0.48$ (from the region of the so-called morphotropic phase boundary, MPB), the strongest piezoelectric properties occur [18]. These PZT materials are used mainly in the form of ceramics, thin films, or multilayers, because of difficulties to grow single crystals. A few years ago, PZT crystals with Ti content $x > 0.1$ were grown [19]. Before, Whatmore et al. [20] were able to grow PZT crystals with Ti content below 0.1 only, and the most

* Corresponding author.
E-mail address: iwona.lazar@us.edu.pl (I. Lazar).

important result of that work was to show the differences between phase diagrams for ceramics and crystals of PZT. Although many reports on the physical properties of single PZT crystals have been published [21-29], it still remains a challenge to grow them over the entire range of Ti content.

We have successfully obtained a compositionally homogenous $PbZr_{0.87}Ti_{0.13}O_3$ (PZT 87/13) single crystal by using the TSSG technique. Structural studies proved that at room temperature, the best crystal structure fit was for monoclinic *Cm* symmetry [26]. The *Cm* space group contains two possible monoclinic phases: M_A and M_B [12]. The size of the obtained crystals allowed for piezoelectric measurements by means of resonance and quasi-static methods. One of the most interesting results of this work is the high value of the piezoelectric coefficient (d_{33} is over 2500 pm V^{-1}) in the new, recently discovered, phase. This additional phase transition is described in ref. [26,30,31]. Here, we report on the high piezoelectric response observed for the PZT 87/13 crystal under a strong external electric field, through a quasi-static method. To explain this intricate phenomenon, optical studies of the optical direction orientations under the influence of strong d.c. electric field were carried out.

2. Experimental

$PbZr_{0.87}Ti_{0.13}O_3$ single crystal with homogeneous composition was grown by top-seeded solution growth (TSSG) technique. The high quality of the crystal was manifested by its density of 7990 kg m^{-3}, very close to the theoretical value [32]. Powder diffraction measurements, conducted on the crushed single crystals at room temperature, revealed the best structure fit for the monoclinic phase, *Cm* [26].

2.1. Piezoelectric measurement by resonance technique

In resonance technique, the $(001)_c$-oriented single crystal bar was cut to required sample geometrical conditions, i.e., the shape of a cuboid [33] (throughout this article, the pseudo-cubic perovskite unit cell is used, and it has been designated as subscript '*c*'). The bases of crystal in cuboid shape, having the dimensions of 2.0 x 0.5 x 0.4 mm^3 were electroded with silver paste. Prior to experiments, the crystal was polarised in d.c. external electric field of the strength of 7 kV cm^{-1} applied at 120 °C, and cooled in this field to 25 °C, at which the field was switched off. For chosen temperatures, the complex admittance $Y=|Y|e^{i\theta}$ in the function of frequency f was measured by Agilent 4192A Impedance Analyzer. The measurements of piezoelectric resonances were carried out with the use of a sinusoidal a.c. electric field of a small intensity, amounting to 0.005 kV cm^{-1}, applied to a previously polarised single crystal. The application of forced harmonic oscillator model to describe admittance changes near the piezoelectric resonance [34] allowed us to determine the parameters needed to calculate the value of the piezoelectric module d_{33}.

2.2. Piezoelectric measurement by quasi-static technique

In the quasi-static technique based on inverse piezoelectric effect, the $(001)_c$-oriented single crystal in the shape of a plate with a thickness of 0.3 mm was electroded with silver paste. An alternating electric field applied to the piezoelectric sample caused deformations recorded by a capacitive sensor. The electric field frequency and strength amounted to 70 Hz and 7 kV cm^{-1}, respectively. One end of the quartz rod was placed on the sample surface, and the other end was connected to the sensor-capacitor plate. The piezoelectric deformation was detected through the measurement of the electric current flowing in the circuit and caused by changes in the sensor capacity [35]. The electric current changes occurring

with temperature changes were measured with the use of SR830 lock-in amplifier. The recorded deformation of the sample along the electric field direction corresponded to the *effective* piezoelectric coefficient d_{33}. The software for this method of measurement made a continuous measurements of d_{33} possible. In this measurement, the crystal was not previously polarised, and the registered signals came from a region of tens of μm^2, located under the quartz rod.

2.3. Birefringence measurement

A multi-domain PZT 87/13 single crystal having the thickness of 300 μm was used in birefringence studies and examination of domain populations. The measurements were performed by means of Oxford Cryosystems Metripol Birefringence Imaging System (Metripol). This system consists of a polarizing microscope equipped with a polarizer capable of rotating to fixed angles α from a reference position, a circularly polarizing analyser and a CCD camera. The sample was held by Linkam THMS600E temperature microscope stage, which maintains a constant temperature to within 0.1 K.

The principle of the measuring technique is that the light first passes through the polarizer. Next, the polarised wave passes through a t-thick anisotropic crystal. Birefringence is the result of anisotropy within the sample, leading to a variation of the refractive index n. This variation is represented by an indicatrix with three principal refractive indices: n_1, n_2, n_3, e.g., ref. [36]. For any given incident light direction, the perpendicular cross-section of the indicatrix will generally have the form of an ellipse. The difference in the lengths of the axes of the ellipse is equal to $\Delta n = n_1 - n_2$. Together with the inclination φ of the indicatrix, it describes the optical retardation Γ within the sample that appears for the particular direction of light [37]. The light intensity I, registered by a CCD camera, can be expressed as: $I = 0.5 \, I_0 \, [1 + \sin(2\varphi - 2\alpha) \sin\delta]$. Here, I_0 is the intensity of unpolarised light passing through the sample, α is the angular position of the analyzer as it rotates, and φ is the angle of principal axis of the indicatrix (optical orientation) with respect to a predetermined position. In our case, φ is defined as the angle measured anticlockwise from the horizontal direction of the microscope stage to the slow (longer) axis of the indicatrix. The difference in refractive index implies that the two orthogonally polarised components have a phase difference of: $\delta = (2\pi/\lambda) \cdot \Delta n \cdot t = (2\pi/\lambda) \cdot \Gamma$ (where the sample thickness is $t = 300$ μm, the used wavelength of the light is $\lambda = 570$ nm). On passing through the birefringent crystal, a beam of linearly polarised light will become elliptically polarised with a phase difference δ and a difference in amplitude depending on the angle φ. In practice, at selected temperatures, we obtain a color map of the $|\sin\delta|$ and φ.

Here is how to find the value of Δn. The measured changes of $|\sin\delta|$ with temperature allow to determine the variation of Γ, at which the maxima of the periodic output signal $|\sin\delta|$ occur, provided that $\Gamma=[(2\ N\ +\ 1)\lambda]/4$, where N is an integer. Hence, the birefringence was calculated using the formula: $\Delta n = [(2\ N\ +\ 1)\lambda]/4t$ [37].

Linkam THMS600E temperature stage also enables heating or cooling of the sample under the electric field. The first thermal cycle has been performed with the electric field of the strength of 7 kV cm^{-1}, followed by a second cycle for the previously polarised crystal. The direction of the applied electric field was along the thickness of the sample, i.e., it was parallel to the incident light direction. The direction of poling in the d.c. external electric field was also parallel to incident light. Such a direction of the electric field in relation to the incident light beam was achieved with a capacitor with transparent electrodes. The birefringence measurements for PZT 87/13 crystal were carried out from 160 °C to

300 °C. Experiments were conducted with the temperature rate of 1 K min^{-1}.

2.4. Dielectric measurement

For dielectric measurements, the same sample as that utilized in optical studies was used. Silver paste electrodes were deposited on a single PbZr$_{0.87}$Ti$_{0.13}$O$_3$ crystal. The capacity C was measured at the frequency of f = 1 MHz using Agilent 4192A Impedance Analyser, on heating, at the rate of 1 K min^{-1}, in the temperature range of $40 - 390$ °C. The real ε part of the permittivity was calculated using the following formula: $\varepsilon = C/C_0$ with $C_0 = \varepsilon_0 \cdot S/t$, where S is the electrode surface, t - sample thickness, and ε_0 is the permittivity of free space.

3. Results and discussion

3.1. Piezoelectric and dielectric properties

Piezoelectricity is an anisotropic property, and it is important to know the symmetry of the studied material. It is not easy in the case of the crystal under consideration. From a recent phase diagram for PZT with Ti content close to x = 0.1 [16], a mixture of the rhombohedral R and monoclinic M$_B$ phases was established. However, the analysis of the X-ray diffraction could not distinguish between the monoclinic phases M$_A$ and M$_B$. According to the eighth-order Devonshire theory by Vanderbuilt and Cohen [12], three possible monoclinic phases: M$_A$, M$_B$, and M$_C$ exist in PZT, although with different probabilities. While M$_A$ is the most probable to appear in perovskite ferroelectrics, M$_C$ and especially M$_B$ may be harder to find in real materials. M$_A$ and M$_B$ belong to the same space group, *Cm*, and M$_C$ to the *Pm* space group. In the context of the current paper, M$_A$ and M$_B$ phases are treated equally. In the beginning, only M$_A$ and M$_B$ phases were observed experimentally in the PZT ceramics [16]. More recent studies proved that the monoclinic phase M$_C$ coexists with M$_A$, and for compositions with Ti content below 50%, the M$_A$ phase dominates (Fig. 3 in ref. [38]). Because the coexistence of M$_A$, M$_B$, and M$_C$ phases makes the polarization vector rotation possible, this leads to the enhancement of piezoelectric properties. The polarization rotation in M$_A$ and M$_B$ was registered at the unit level in Zr-rich PZT 75/25 [39]. The electromechanical properties of a single crystal constitute a multi-faceted issue, because the symmetry of the PZT depends on the length scale considered [40]. Therefore, in this paper, the piezoelectric properties have been investigated on crystals using two different methods. While the resonance method registers the macroscopic response of a polarised crystal, the quasi-static method gives a piezoelectric response from the area of dozens of square-microns and at much higher electric field action.

It was found that the (001)$_c$-oriented single crystals of oxide ferroelectrics exhibit a high k$_{33}$ electromechanical coupling coefficient, and piezoelectric coefficient d$_{33}$, due to domain-engineered effects [41,42]. In these domain-engineered oxide ferroelectrics, the direction of polarization differs from that of the dipoles in individual unit cell and a multi-domain structure is created, i.e., the polarization vector is not parallel to Z-direction. Gorfman et al. [43] showed that in multi-domain PZT 65/35 crystal, domain wall motions have a slightly higher contribution to the total piezoelectricity than the part deriving from changes in lattice parameters. The crystal configuration selected for the research corresponds to the expected optimal piezoelectric response.

In the quasi-static method, strain η_3 was measured in the direction of the applied a.c. electric field E$_3$ and the equation for inverse piezoelectric effect, $\eta_3 = d_{33} \cdot E_3$, was applied (Fig. 1a). To measure d$_{33}$ by resonance method, the crystal must have a size configuration as provided in Fig. 1b. In resonance technique, when an a.c.

electric field of a small amplitude is applied to a polarised single crystal, large amplitude oscillations occur near resonance frequencies. A disadvantage of this technique is that a relatively large sample is required, but the obtained single PbZr$_{0.87}$Ti$_{0.13}$O$_3$ crystal was large enough to suit such requirements. The dielectric characteristics (Fig. 1c) distinguishes at least the main temperature point at 275 °C. Fig. 1d represents the linear dependence η_3(E$_3$), from which coefficient d$_{33}$ has been calculated. The d$_{33}$ values obtained by those two different methods are close to each other only in the temperature range below 195 °C (inset in Fig. 1e). When the crystal was heated above 195 °C, the piezoelectric response of the crystal in a strong (red dots in Fig. 1e) and a weak (blue dots in Fig. 1e) electric field differ substantially. It should be remembered that the resonance method registers the macroscopic response of a polarised crystal (blue dots in Fig. 1e) in which polarization is oriented on the average in the Z–axis direction. Low electric field strength is applied to induce piezoelectric resonances. Such a small field certainly does not cause any domain wall movements or domain reorientations. In opposite to the resonance method, the quasi-static technique gives a piezoelectric response from an area of dozens of square-microns and for a much higher field. This strong measuring electric field affects the domain structure of the crystal and directions of polarization vector. Hence, we can assume that the drastic increase of the d$_{33}$ value above 195 °C has to be related to the rotation of the polarization vector in this external electric field. This rotation is easily realized in unit cells of the monoclinic symmetries. Between M$_A$ and M$_B$, the polarization vector rotates in one plane. Moreover, the appearance of the M$_C$ phase allows the polarization vector to turn in different planes [25]. However, we cannot exclude an additional contribution to the piezoelectric response made by domain wall movements under the electric field. Such share of the domain wall reorientations is reported in [43]. Interestingly, the d$_{33}$ can immediately reach the immense value of 2500 pm V^{-1}, which subsequently irregularly diminishes to 0 when approaching 250 °C. It is worth noting that an additional anomaly, a hump on the ε(T) run, was observed around this temperature (Fig. 1c). Finally, the crystal becomes piezoelectrically inactive at around 280 °C, i.e., at a temperature slightly higher than that related to a maximum of ε(T). It is comprehensible if only the influence of an external electric field is taken into account. These remarkable piezoelectric results have been obtained in the range of temperatures which corresponds to a new phase, recently discovered in Zr-rich solid PZT solutions [26,30,31]. It results from the above that we can suspect the polarization vector rotation (and also domain structure dynamics) to be the leading cause of that unusual behavior of piezoelectric properties. To verify this assumption, optical studies of the virgin crystal, crystal poled in d.c. electric field, and crystal under the continuous action of d.c. electric field have been performed.

3.2. Optical observations of domain structures in virgin crystal

In such optical studies, most often the angle between polarization directions in the adjacent domains is considered. For example, there are 90° or 180° domains in the tetragonal T phase and 71° or 109° domains in the rhombohedral R phase [44]. In the first case, the extinction directions of domains are compatible with the orientations of the optical indicatrix (i. e., $\varphi = 0°$ or 90°), and in the second one they are not [Fig. 2b in ref. [25]. Below, we present the results of investigations of temperature changes of the optical indicatrix orientations (responsible for extinction directions) characterizing the structure coexistence. As described above, the measure of this orientation is the φ angle. In our case, φ (optical orientation) is defined as the angle measured anticlockwise from the horizontal direction of the microscope stage to the slow (longer) axis of the indicatrix.
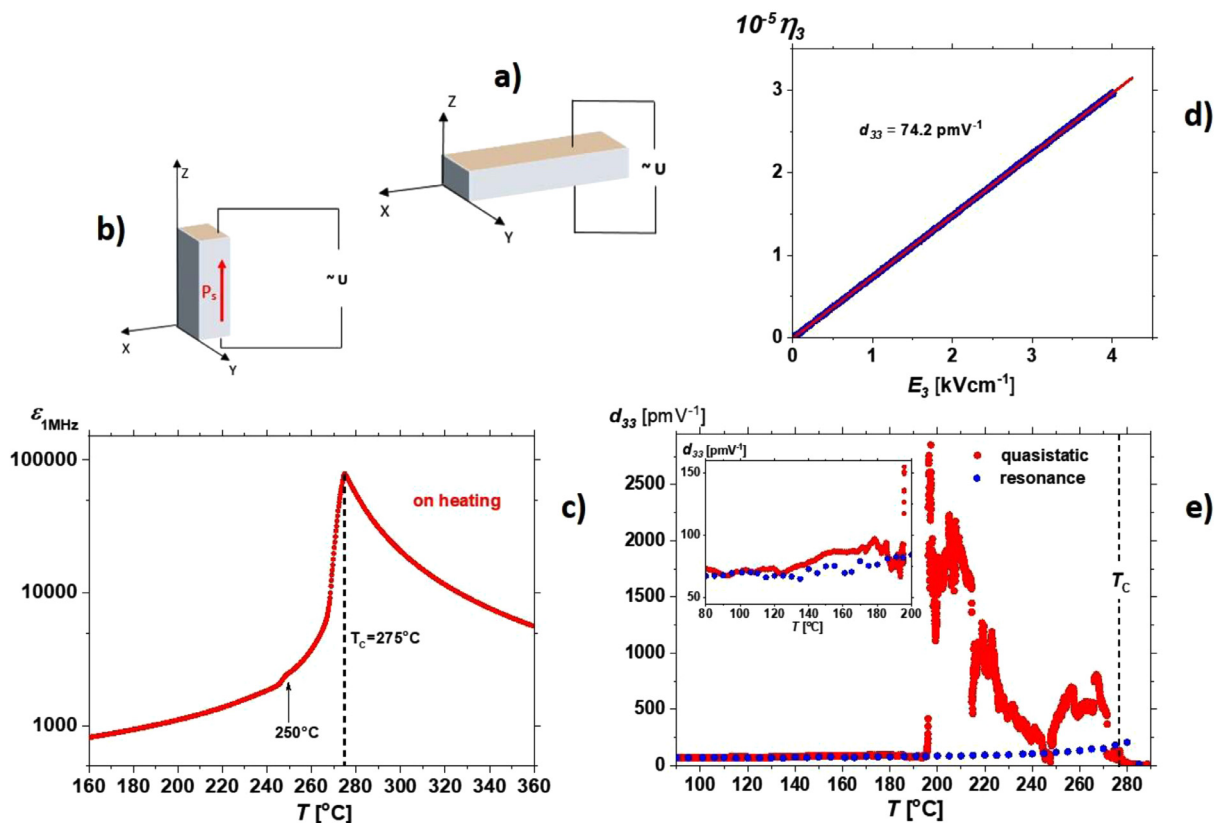
Fig. 1. Geometric configurations of crystals for measurements of piezoelectric coefficient d_{33} by **a)** quasi-static and **b)** resonance techniques. **c)** Temperature dependence of permittivity ε_{1MHz} in logarithmic scale measured for a PZT 87/13 crystal on heating. Note that there is no anomaly at a temperature at which d_{33} dramatically increases in the quasi-static method. The black arrow shows a small hump connected with reorganization in domain structures (see further in the text). **d)** Room temperature piezoelectric response of a single $PbZr_{0.87}Ti_{0.13}O_3$ crystal determined by quasi-static method. The value of d_{33} was determined from the slope of the straight line and amounted to 74.1 pm V^{-1}. For crystal thickness of $t = 300$ μm and for electric field of $E_3 = 4$ kV cm^{-1}, the strain η_3 along Z-direction was equal to $\eta_3 = d_{33} \cdot E_3 = 3 \cdot 10^{-5}$, and thus the maximum of the amplitude of crystal deformation in this experiment was determined as $\Delta t = \eta_3 \cdot t = 9$ nm. **e)** Piezoelectric coefficient d_{33} as a function of temperature, for a PZT 87/13 crystal in a weak (in blue) and strong (in red) electric field. The inset concerns the temperature range in which $d_{33}(T)$ runs are similar.

It has already been shown that PZT single crystals have complex domain structures over a wide temperature range and various compositions, even far away from the MPB [25,27]. Optical studies, as that for perovskite crystal $Na_{0.5}Bi_{0.5}TiO_3$ [45], showed a broad angular distribution of optical orientations, without clearly visible crystallographically oriented domain walls, which characterizes the coexistence of phases of different symmetries. It has already been accepted that the symmetry of the PZT depends on the length scale considered [40]. On the local length scale, the monoclinic symmetry in the PZT applies to almost all compositions. Still, on a larger scale, this symmetry appears only in the compounds close to the MPB. That is why optical studies of a single $PbZr_{0.87}Ti_{0.13}O_3$ crystal have been carried out in the temperature range where the most interesting piezoelectric behavior has been observed. At chosen temperatures, the optical orientation populations have been analyzed to discriminate the temperature-dependent contribution of all phases present in the crystal. In the uniaxial rhombohedral phase, the 45° and 135° orientations of the optical indicatrix are observed. In contrast, in biaxial monoclinic M phase, two cases have to be considered: i) the monoclinic phases of Cm can be distinguished from M_C by the fact that in the Cm phase, there are 45° but no 0° orientations, ii) according to [25,46], in M_C there are 0°, but 45° orientations do not exist. Other orientations in monoclinic phases may also occur, including those of micrometer size, depending on the composition and temperature [25]. The local R and M symmetries were observed in Zr-rich PZT, whose directions depended on temperature [39]. The application of our experimental technique allowed to observe domain orientations through the measurement of extinction angle, φ [37]. Fig. 2 shows the method of determining this angle for the area inside one domain. Since our technique allows to measure the $|\sin\delta|$, its characteristic feature is that φ changes by 90° every time $|\sin\delta|$ goes through zero, thus appearing to be alternately assigned to the fast and to the slow axes [37]. Therefore, for example, for the rhombohedral phase, we can obtain two values of φ: 45° and 135°. This angle is measured in reference to $[100]_c$ direction.

As shown in Fig. 3, in virgin PZT crystal the domains with $\varphi=45°$ and 135° exist up to the phase transition point. However, these domains appear in both the R and Cm phases. A contribution of domains derived only from the monoclinic Cm (M_A and M_B) phase is visible as additional maxima for angles 55° and 32° in Fig. 3, for 180 °C. This study could not distinguish which domains come from the M_A and which from the M_B structure. According to the paper by Vanderbilt and Cohen [12], the M_A phase is more probable to appear, but in the report [16], the appearance of M_B phase is referred to as more likely. In the ceramics with similar composition as in the studied crystal, both structures were observed [39]. The presence of the Cm symmetry for the crystal of this composition is not surprising as it has already been found at room temperature in recent structural studies [26]. Nevertheless, the presence of 0° (very little) and 90° optical orientations, proving the existence of a monoclinic M_C structure, may come as a surprise. Previously, the M_C phase in PZT with a low concentration of Ti had not been reported. In optical studies, the existence of a Pm (M_C) phase is questionable because the only report
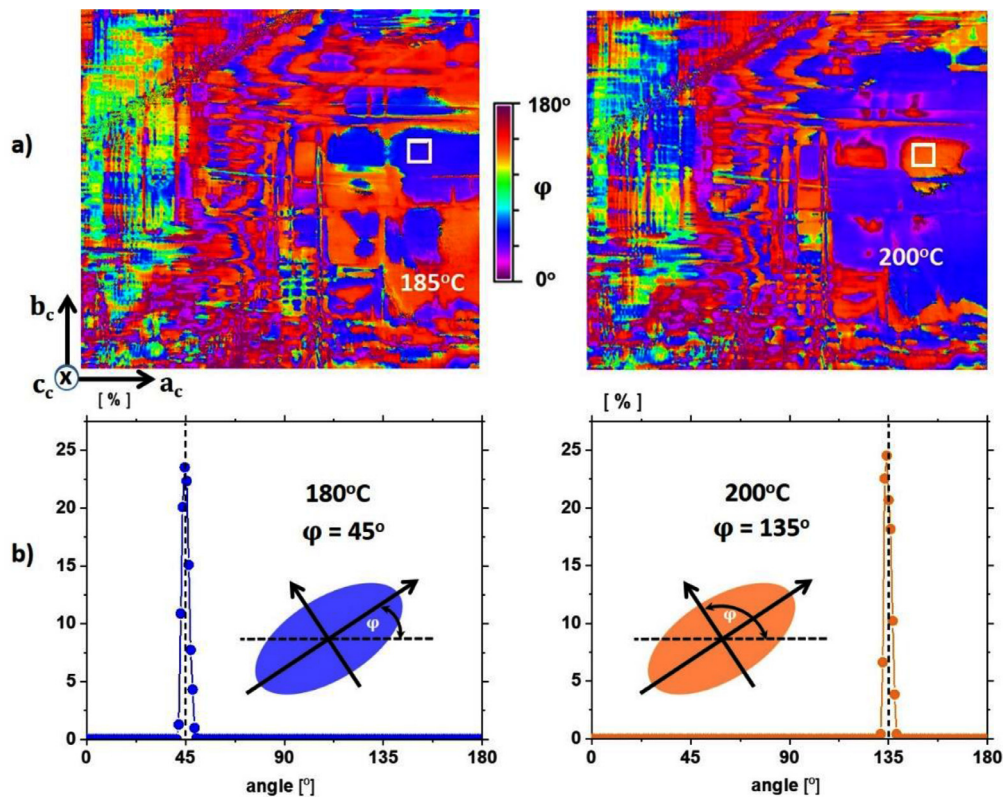
Fig. 2. a) The figures show changes in the map of the extinction angle φ for two chosen temperatures. Symbols a_c, b_c and c_c denote axes of the pseudo-cubic unit. The blue and orange colors, marked by a white rectangle, describe the R phase, and they can also come from the *Cm* phase. The size of domain changes with temperature, i.e., the selected orange domain is smaller than the blue one; however, the white rectangle always lays inside the same domain, to illustrate the experimental technique used. **b)** The calculated domain population assumes the same value. Some distribution of signals is connected with the sensitivity of the method used. The data are taken from the region marked by the white rectangle (35 μm x 30 μm) at 180 °C and 200 °C. .

of a M_C structure in the literature [38] is a paper on PDF (thus in the atomic scale) of PZT near the MPB. That is why we cannot definitively confirm the *Pm* (M_C) phase, based only on the optical studies. Another feature is the fit of Gaussian lines for M_C orientations (Fig. 3) which have a substantial full width at half maximum (FWHM). Statistically, this gives many optical orientations with the low intensity that build the characteristic 'background' in the whole range of angles (a broad Gaussian line with an expected value of the extinction angle equal to 90°, magenta line in Fig. 3). It is also possible that several domains stay on top of each other, affecting the average optical indicatrix section [45]. It is important that for rhombohedral and tetragonal domains, the extinction angle value does not change (or changes only by 90°). With increasing temperature, the histograms become sharper (Fig. 3), indicating a decrease in possible optical orientations and a growth in domains. Above 230 °C, the 'background' disappears, and at 240 °C, the PZT 87/13 crystal still features the R and *Cm* (M_A and M_B) phase coexistence. There is a significant growth of the *Cm* phase - except for the two peaks around 45°, a high line for an angle of less than 135° (yellow line) appears. These changes may cause the above- mentioned minor anomaly on the ε(T) run in Fig. 1c. Above 240 °C, there is coexistence of R and *Cm* phase, which is observed up to 270 °C. The slight number of 0° and 180° optical orientations seen at 280 °C is connected with the experimental sensitivity (optical resolution) of the setup used.

Because of the high number of possible extinction directions in the M phases (up to 24) [12], a division of crystal volume into small territories of these phases in lower temperatures provides more lines and wider ones as well. This broad distribution of optical orientations may also be due to the overlap of different domains. Such a broad range of optical directions ('background') was reported in [45] as coming from overlapping monoclinic domains of different thickness.

3.3. Optical observations of domain structures under d.c. electric field

Figs. 4 and 5 represent changes of optical direction populations under the influence of d.c. electric field for the same region as that marked by the white rectangle in Fig. 3. These changes are caused by rotation of polarization vector in the electric field, accompanied by modification of the population of optical orientations. At 180 °C, a small population at 135° (the dark yellow line in Fig. 4 and red dots in Fig. 5) shows a change in the polarization vector direction in the R and Cm phases under the electric field - the population at 45° (blue line in Fig. 4) increased. The absence of these lines at 200 °C and 210 °C (Fig. 4) testifies to the disappearance of the R phase, in place of which the monoclinic phases appear, with wide range of φ angle value. The analysis of domain pattern in d.c. electric field (Fig. 4 and red dots in Fig. 5) shows that the contribution of the small domains population and dense domain walls (red and magenta lines) has increased and is visible even at 280 °C. However, at 240 °C, the 'background' decreases significantly, and the R phase lines (blue at 45° and dark yellow at 135°) reappear. Under the electric field action, this selected area of the crystal is still locally ferroelectric, even at 280 °C.

Here, it is worth mentioning that local Pb displacement from Z-direction defines the polarization vector in the M phases (Fig. 6c). Thus, one can state that in the PZT 87/13 crystal exposed to d.c. electric field, the monoclinic phases coexist in the temperature range of 180–280 °C. In the temperature range of 200–210 °C (the highest values of d_{33} were recorded there), the change in symme-
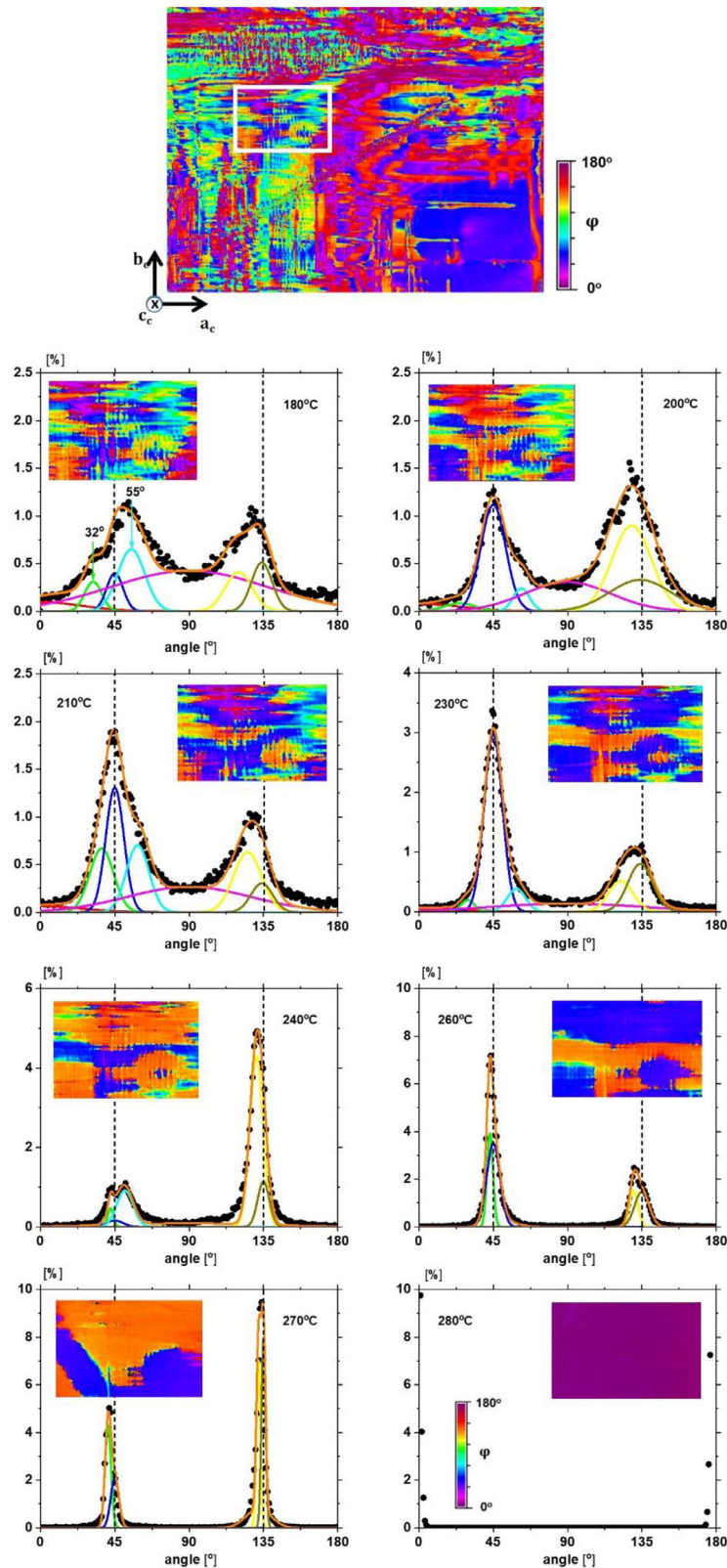
Fig. 3. The upper figure with a white rectangle of 250 μm x 130 μm presents a region at 180 °C for which the distribution (histogram) of optical directions in the $(001)_c$ crystalline plate of virgin PZT 87/13 crystal has been calculated. It is the region for which the quasi-static piezoelectric signals were detected (Fig. 1e). Histograms for the selected eight temperatures show changes in the content of different phases. Insets represent maps of the φ angles of optical indicatrix. Continuous Gauss-type lines are fits showing possible extinction angles. The dotted perpendicular lines mark angles: $\varphi = 45°$ and $\varphi = 135°$ occurring in the rhombohedral, R, and monoclinic, Cm, phases. For example, at 180 °C, the angles of 32° (in green) and 55° (in cyanine) are also observed, which are characteristic only for the Cm (M_A and M_B) phase; the broad and flat lines for 0° (in red) and 90° (in magenta) angles mainly form the characteristic 'background' mentioned above. With an increase in temperature, the distribution moves towards the coexistence of R and Cm phases. The origins of differences in populations for $\varphi = 45°$ and 135° domains are the experimental features shown in Fig. 2. The homogenous map in dark magenta at 280 °C corresponds to the paraelectric phase. Note the different scales of [%] axis.
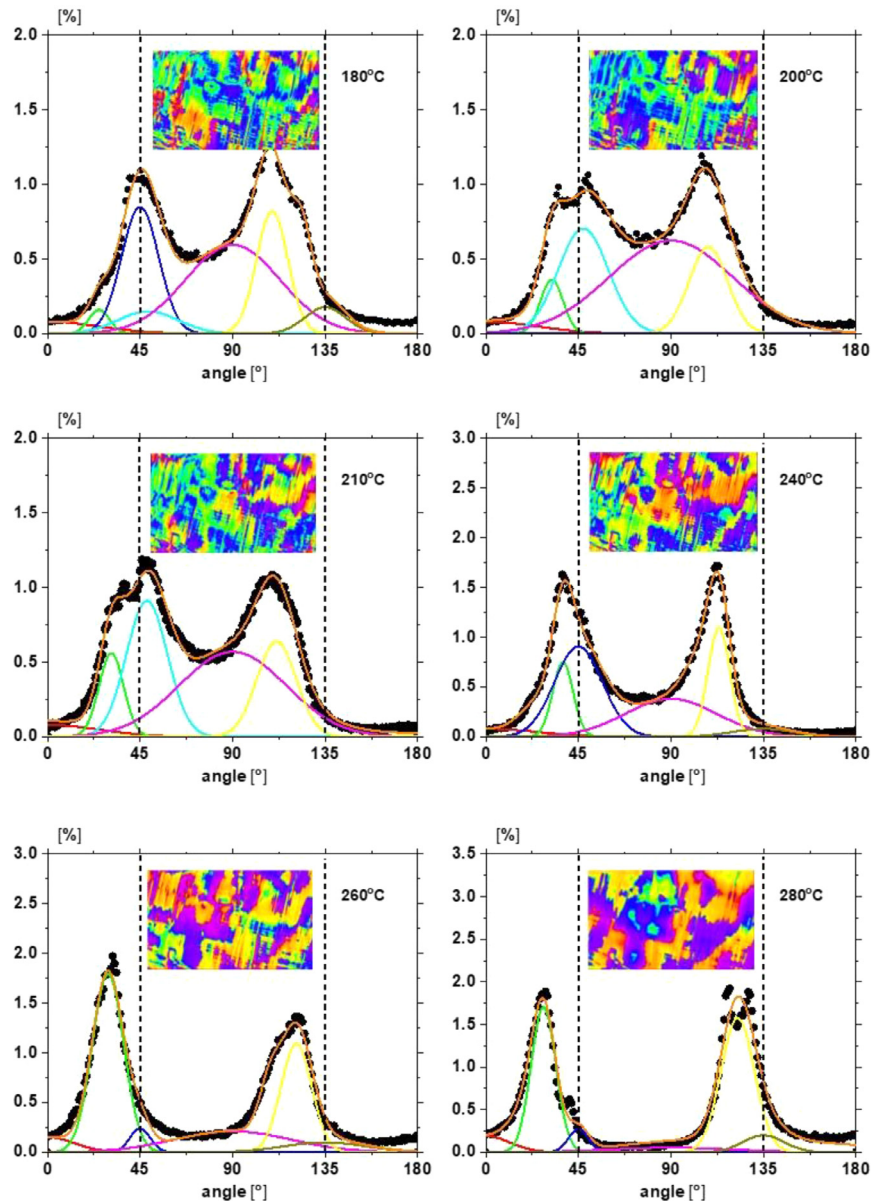
Fig. 4. Optical orientation populations at selected temperatures in the $(001)_c$ crystalline plate for PZT 87/13 single crystal under d.c. electric field of 7 kV cm^{-1}. Insets show the maps of optical indicatrix orientations. The angles 45° and 135°, characteristic for the R and *Cm* phases, are shown by black dotted lines. Angles 0° (in red) and 90° (in magenta) come from the already mentioned 'background', and are visible better than in Fig. 3 (without the E field). Note that at 200 °C and 210 °C, there are no lines for angles 45° and 135° (these lines are shown in blue and in dark yellow, respectively, in other histograms). .

try from R to M under d.c. electric field causes changes in the optical orientation populations. In such complicated structures, the movement of domains and domain walls has to be influenced by the action of electric field. This movement has to have a share in crystal strain and can be treated as an extrinsic contribution to the piezoelectric effect [47].

The piezoelectric properties presented in Fig. 1e distinguish two temperature regions. The first one, below 195 °C, in which the d_{33} coefficient measured by two different methods has the same value. The second one, above 195 °C, in which the increase and irregular changes of d_{33}, measured with the quasi-static technique, are visible. Below 195 °C, in virgin crystal, R and M phases coexist (Fig. 3 at 180 °C), while in the electric field, a much higher content of M phases occurs (Fig. 4 and 5). The absence of the R phase in a strong electric field (for 200 °C and 210 °C in Fig. 4) corresponds to the temperature range of the highest value of piezoelectric coefficient d_{33}, measured in a strong E field by quasi-static method

(Fig. 1e). This is because strong electric fields can cause the polarization vector rotation between different phases (Fig. 6c), which implies the most significant change in the polarization value, and thus the highest piezoelectric response. Moreover, when the background is present and consists of small domains with dense domain walls, it enhances the values of the piezoelectric coefficients.

It is also worth recognizing that close to 250 °C, the d_{33} disappears in the quasi-static method (red dots in Fig. 1e). To explain this effect, we studied the evolution of optical orientation populations with temperature. The calculation of phase populations in crystal with no E field action (Fig. 6a) shows that a single peak (around 45°) at 230 °C, mainly corresponding to the R and *Cm* phase populations, splits into two smaller peaks at 240 °C (Fig. 3), which mostly correspond to *Cm* phase populations. At the same time, the populations for the angle smaller than 135° (Fig. 3) have increased significantly at 240 °C. Above 240 °C, the orientations around angle value of 45° dominate again. However, under
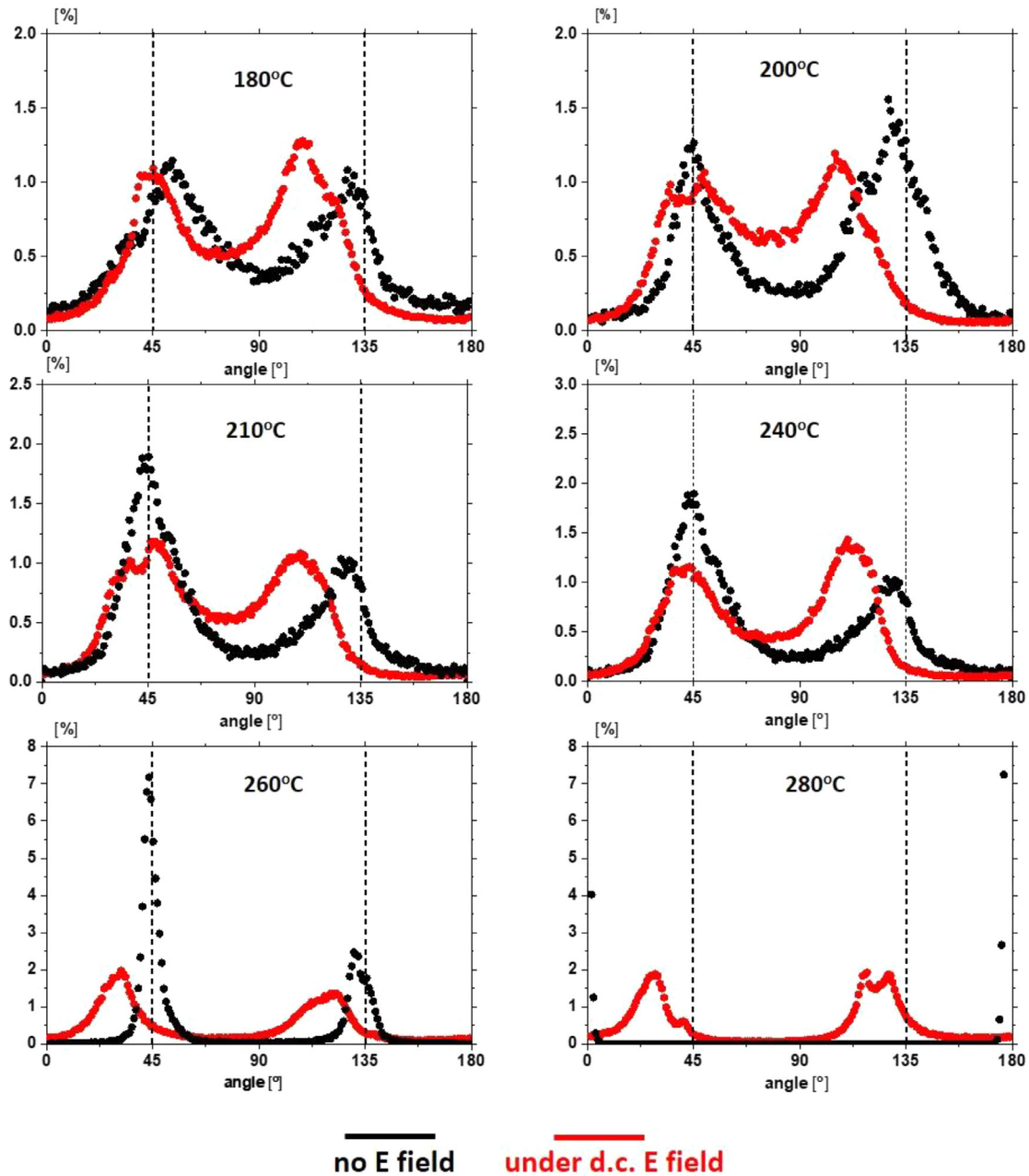
Fig. 5. Comparison of optical orientation populations at selected temperatures in the $(001)_c$ crystalline plate for PZT 87/13 single crystal. With no E field (in black) and in d.c. electric field 7 kV cm^{-1} (in red). Note the different scales of [%]. The shift of local maxima of optical orientation populations under d.c. field testifies to the rotation of polarization vector in the monoclinic unit cell with temperature. The angles 45° and 135°, characteristic for the R and *Cm* phases, are shown by black dotted lines.

the influence of an electric field, these optical orientation populations characteristic for the R and *Cm* phases (around 45° and 135°) are significantly reduced (Fig. 6b). Interestingly, the characteristic 'background' drops much above 240 °C (Fig. 4). Comparing Figs. 6a and 6b, it can be noted that the presence of electric field has increased the monoclinic phase populations. Populations in Fig. 6b have decreased (note different scales on ordinate axes in Figs. 6a and 6b) and - at the same time - the peaks become smaller and broader because of the increase in the number of possible directions of extinctions in M phases (up to 24). This wide optical orientation distribution can also come from the overlapping of different domains. Consequently, such an arrangement of domains of several phases may result in local disappearance of piezoelectricity in the crystal.

3.4. High-temperature birefringence in PZT 87/13 crystal

Birefringence studies have been performed to explain the unexpected disappearance of piezoelectric activity at around 250 °C (Fig. 1e). Although the whole studied crystal contains complex domain structures, finding an appropriate area of 25 μm x 35 μm inside a single domain was possible. Fig. 7a shows the Δn(T) dependence for three different states of the crystal (inset on Fig. 7a shows an area for which the birefringence Δn has been calculated). While a shift of the transition point T_C to paraelectric phase towards higher temperatures under d.c. E field action is an expected behavior, T_C higher than in crystal after polarizing is not such an obvious effect. It either indicates the existence of internal random fields that maintain a polarised state, or it means that
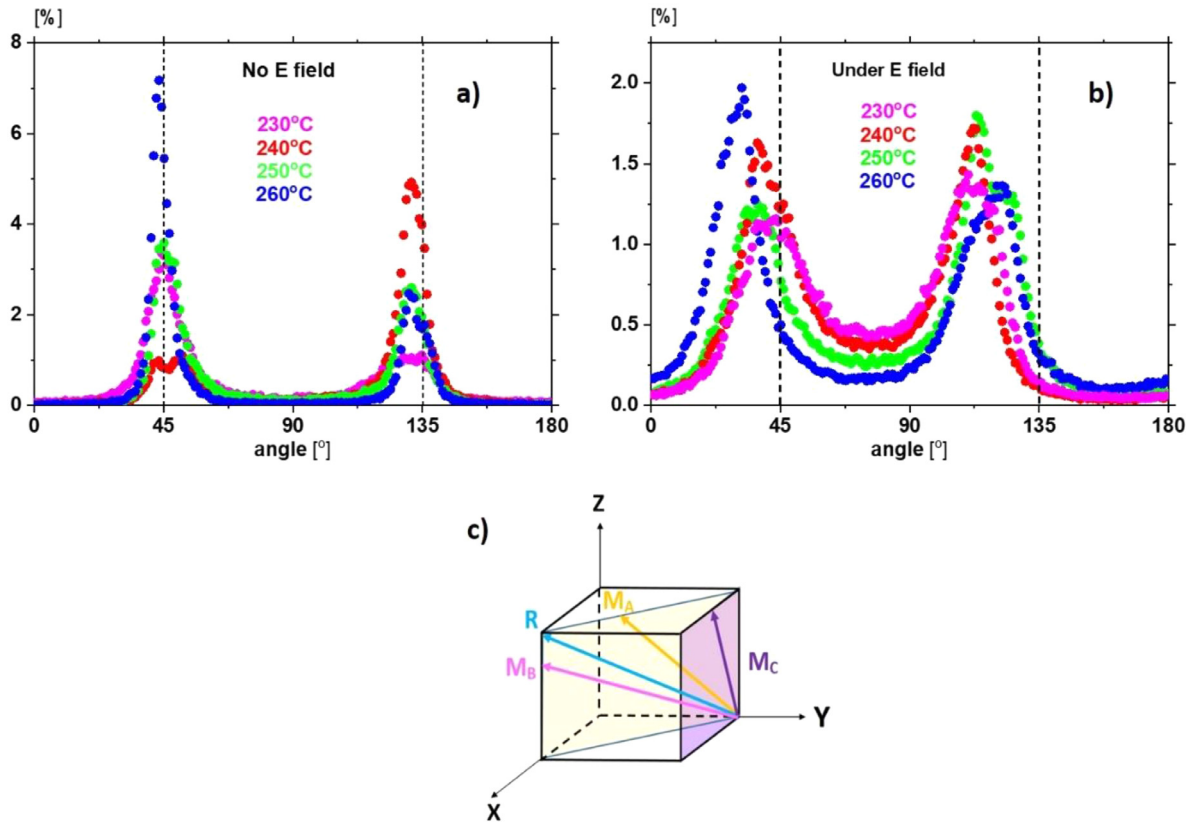
Fig. 6. Temperature evolution of optical orientation populations at selected temperatures in the (001)$_c$ crystalline plate of PZT 87/13 single crystal in the range of 230–260 °C: **a)** virgin crystal, and **b)** crystal under E field (note the different scales of [%] axis). **c)** directions of polarization vector in monoclinic phases: M$_A$, M$_B$, M$_C$, and rhombohedral R phase. .
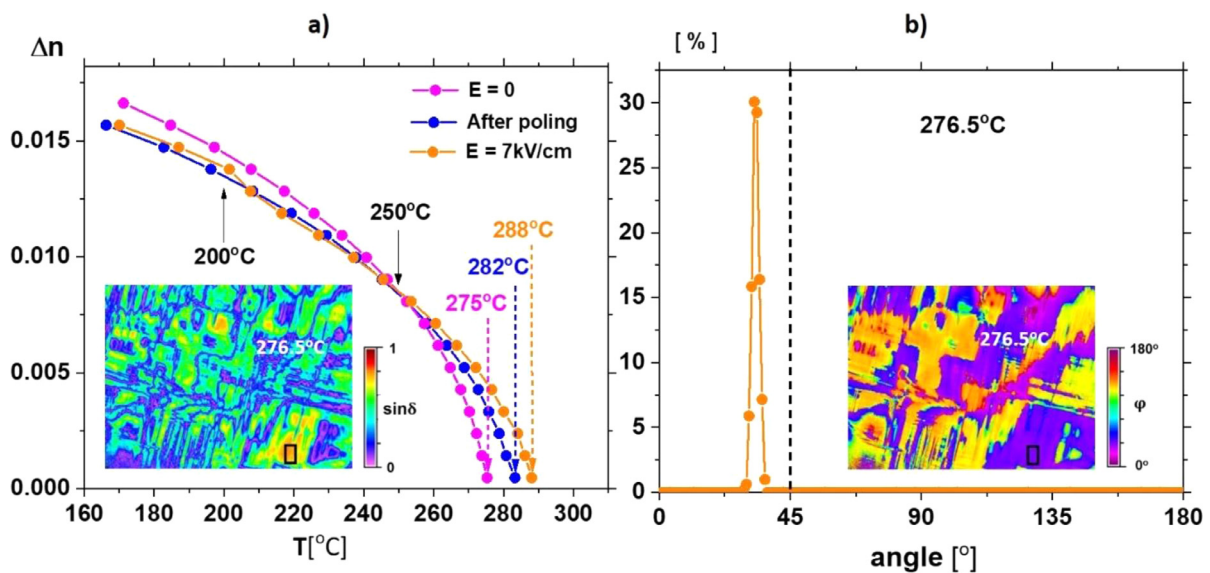

Fig. 7. a) Change of birefringence, $\triangle$n, with temperature for the PZT 87/13 single crystal: virgin state (magenta), polarised crystal (blue), and crystal under the permanent action of d.c. electric field (orange). $\triangle$n values have been calculated for an area of 25 μm x 35 μm inside one domain, marked by the black rectangle in the inset. **b)** Optical orientation populations for the studied region in the crystal under the action of d.c. field. The angle value of 32° corresponds to monoclinic Cm phase. The black dotted line marks the 45° angle characteristic, among others, for the R phase. It has been found that the electric field of E = 7 kV cm^{-1} does not influence the calculation of $\triangle$n value because of induced piezoelectric deformation; for a crystal with the thickness of 300 μm, even the piezoelectric coefficient value of d$_{33}$=3000 pm V^{-1} changes the thickness by no more than 0.6 μm, and thus can be neglected.

Table 1
The symmetries considered so far for ferroelectric PZT.

Symmetry	Piezoelectric matrix [43]	Space group	Spontaneous polarization direction [12]
cubic (C)	$\begin{pmatrix} 0 & 0 & 0 & 0 & 0 & 0 \\ 0 & 0 & 0 & 0 & 0 & 0 \\ 0 & 0 & 0 & 0 & 0 & 0 \end{pmatrix}$	$Pm\bar{3}m$	
tetragonal (T)	$\begin{pmatrix} 0 & 0 & 0 & 0 & d_{15} & 0 \\ 0 & 0 & 0 & d_{15} & 0 & 0 \\ d_{31} & d_{31} & d_{33} & 0 & 0 & 0 \end{pmatrix}$	$P4mm$	$<100>$
rhombohedral (R)	$\begin{pmatrix} 0 & 0 & 0 & 0 & d_{15} & 2d_{22} \\ -d_{22} & d_{22} & 0 & d_{15} & 0 & 0 \\ d_{31} & d_{31} & d_{33} & 0 & 0 & 0 \end{pmatrix}$	$R3m$	$<111>$
orthorhombic (O)	$\begin{pmatrix} 0 & 0 & 0 & 0 & d_{15} & 0 \\ 0 & 0 & 0 & d_{24} & 0 & 0 \\ d_{31} & d_{32} & d_{33} & 0 & 0 & 0 \end{pmatrix}$	$Amm2$	$<011>$
monoclinic (M_C)	$\begin{pmatrix} d_{11} & d_{12} & d_{13} & 0 & d_{15} & 0 \\ 0 & 0 & 0 & d_{24} & 0 & d_{26} \\ d_{31} & d_{32} & d_{33} & 0 & d_{35} & 0 \end{pmatrix}$	Pm	between directions (O) and (T)
monoclinic (M_A)	$\begin{pmatrix} d_{11} & d_{12} & d_{13} & 0 & d_{15} & 0 \\ 0 & 0 & 0 & d_{24} & 0 & d_{26} \\ d_{31} & d_{32} & d_{33} & 0 & d_{35} & 0 \end{pmatrix}$	Cm	between directions (T) and (R)
monoclinic (M_B)	$\begin{pmatrix} d_{11} & d_{12} & d_{13} & 0 & d_{15} & 0 \\ 0 & 0 & 0 & d_{24} & 0 & d_{26} \\ d_{31} & d_{32} & d_{33} & 0 & d_{35} & 0 \end{pmatrix}$	Cm	between directions (O) and (R)
triclinic (Tr)	$\begin{pmatrix} d_{11} & d_{12} & d_{13} & d_{14} & d_{15} & d_{16} \\ d_{21} & d_{22} & d_{23} & d_{24} & d_{25} & d_{26} \\ d_{31} & d_{32} & d_{33} & d_{34} & d_{35} & d_{36} \end{pmatrix}$		between M directions

poling, as well as d.c. E action, changes the crystal local symmetry and shifts the transition point temperature T_C locally (see phase populations at 280 °C in Figs. 4 and 5).

Fig. 7a shows the birefringence measurement Δn in relation to temperature for a virgin crystal, a polarised one, and a sample under the permanent action of the electric field. Virgin sample has the highest Δn values below 250 °C. Up to 200 °C, the birefringence for the polarised crystal is the lowest. Around 200 °C, the Δn values become equal for polarised crystal and crystal under d.c. electric field. Note that we have observed a significant increase in the d_{33} value at around this temperature (red points in Fig. 1e). Interestingly, at 250 °C, three $\Delta n(T)$ dependencies in Fig. 7a intersect at one point, where d_{33} tends to zero in the case of quasi-static technique applied (Fig. 1e). The $\Delta n(T)$ curve obtained under d.c. E field runs below (200 °C $<T<$ 250 °C) and then above ($T>$ 250 °C) the graphs obtained for the other two cases. The linear electro-optical Pockels effect may explain that. The electric-field-induced birefringence is described by the relation $\Delta n_{Poc} = r_{kj}E_j$, where the electro-optical coefficients r_{kj}, are, like piezoelectric coefficients, different from zero in the crystal that lacks inversion symmetry (both coefficients are third order tensors). The electro-optical coefficient changes its sign from positive to negative at around 250 °C. It would mean that at this temperature, r_{kj} assumes the value of zero, and the Pockels effect disappears. It looks as if the crystal had a center of symmetry or it has symmetry in which the respective electro-optical r_{33} and piezoelectric d_{33} coefficients vanish. Of all possible symmetries considered so far for the PZT (see Table 1 below), piezoelectricity disappears only in the cubic phase. A possible scenario is that a strong electric field causes a change in the direction of the polarization vector, in such a way that the crystal observed in the direction of the pseudo-Z-axis is no longer piezoelectric. Table 1 shows that there are many shear piezoelectric coefficients which equal to zero, and the existence of a distinct 'background' presented in Figs. 4 and 6b – being an evidence of large population of the monoclinic phases – would support this explanation.

This scenario may explain the disappearance of piezoelectric activity at 250 °C, presented in Fig. 1e. A strong enough electric field

may induce many different orientations of polarization vector and may make another piezoelectric coefficient active, e.g., the shear mode. It would mean that polarization vectors are oriented randomly for a particular electric field strength in such a way that the piezoelectric effect disappears. In our experiments, it happened at 250 °C. This temperature could be treated as an isotropization point, i. e., the temperature at which a small crystal region appears to have centrosymmetric symmetry in sufficiently strong E field.

The role of shear piezoelectric effect and the presence of complex phase structures seems to be responsible for the unexpected piezoelectric behavior shown in Fig. 1e. In the theoretical work by Bellaiche [48] it was proved that the application of E field along Z-direction to rhombohedral PZT causes the appearance of triclinic or monoclinic structures. The latter phases exhibit enormously high piezoelectric shear coefficients. Such a large piezoelectric response is driven by the electric field induced polarization vector rotation. Theoretical calculations showed that high d_{15} shear coefficient values and induction of monoclinic phase occur when $E = 1000$ kV cm^{-1} [48]. Guo et al. used $E = 20$ kV cm^{-1} [14], while Zhang et al. the $E = 14$kV cm^{-1} [47] and they have proved that in strong electric fields it is possible to induce different phases in PZT, and thus different possibilities exist of polarization rotation, and different piezoelectric coefficients emerge. We applied a lower electric field than in the cited works, but at a higher temperature, i.e. close to a newly reported phase where the perovskite octahedra start rotating in a disordered manner [30]. Such instability makes it easier to induce different phases in the PZT. Therefore we could measure not only the piezoelectric module d_{33}, but others, such as shear piezoelectric coefficients. In the triclinic phase, all piezoelectric modules are non-zero, and therefore in our case, the induction of the triclinic phase can be ruled out [49] (then piezoelectricity would not disappear at 250 °C).

The influence of shear piezoelectric coefficients would thus have an essential role share in the drastic jump of piezoelectric response at 195 °C. For example, the shear moduli d_{34} and d_{36} are inactive in the rhombohedral and monoclinic phases, but are active when the polarization vectors have a direction different than that along the Z-axis. The considered coefficients can be activated when

the field along the pseudo-cubic Z-axis is applied, just as in our experiment. The existence of monoclinic phases and easy changes of polarization orientations in these symmetries, driven by electric field (Figs. 3-5), would make not only these d_{34} and d_{36} coefficients active. Hence, the irregular piezoelectric response above 195 °C seems to be understood.

If the number of domains is statistically large enough, the system is assigned macroscopically to pseudo-tetragonal symmetry (*4mm*) with only three independent piezoelectric coefficients (Table 1). It was shown that the piezoelectric properties of the domain-engineered single crystal increased with the decrease in the domain size [42,50]. A high density of domain walls with spacing in the micrometer range can result in up to a fourfold enhancement of piezoelectricity in $BaTiO_3$ [42]. Moreover, it was found that the [001] poled (*3m*) crystals hold the highest level of stable macroscopic polarization [51], where there are four equivalent directions of the spontaneous polarization vector. The poling electric field is applied along a nonpolar direction, and such a structure is macroscopically polar (has non-zero net polarization). The fibrous domain structure of domain-engineered PZN-PT crystal was composed of the domains that are 130 μm long and about 1 μm wide [52]. These fibrous domain structures contain numerous domain walls, which also contribute to piezoelectricity [44]. We assume that this is one of the possible causes of the increased piezoelectricity observed in the Zr-rich PZT. Gorfman et al. [43]. showed that in the multi-domain PZT 65/35 crystal, domain wall motions make a slightly higher contribution to the total piezoelectricity than the changes in lattice parameters. Simultaneously, it was found that this contribution related to changes in the lattice parameters in individual domains is almost twice as significant. Each domain is surrounded by other domains and remains under mechanical stress imposed by its neighbors. The domain deformation depends not only on the piezoelectric coefficient of the material, but also on the deformation of neighboring domains. These interactions between domains can be constructive as well destructive. These processes are particularly important for crystals with phase coexistence, such as in the investigated PZT 87/13 crystal. The complex coexistence of the rhombohedral and monoclinic phases decides about the magnitude of piezoelectric properties [24,39].

The domain wall charge and its influence on piezoelectric properties should also be taken into account. The incomplete compensation of the associated polarization charge creates a depolarizing field in each domain, leading to enhancement of electromechanical response. For ferroelectrics with a few microns wide domains, depolarizing field of 10–20 kV cm^{-1} was determined [50]. This depolarizing field may be a key factor responsible for the rotation of polarization vector, especially in a complex structure with phase coexistence. It is widely accepted that the monoclinic distortion is recognized as one of the most significant contributors to the high piezoelectric response, especially in a polarization rotation model. In $BaTiO_3$ the d_{33} value was registered as maximum along non-polar axis only in a narrow temperature range, in the vicinity of the tetragonal–orthorhombic phase transition temperature [53]. When a single crystal is poled along non-polar axis, it adopts a multi-domain structure. According to Damjanovic [50], domain wall motions do not necessarily increase the piezoelectric response, but rather the presence of domain walls modifies the material and improves its properties.

This paper has shown that a drastic increase in piezoelectric activity above 195 °C can be explained by the complex domain structures and dense domain walls due to phase coexistence. All mechanisms mentioned above can be considered to explain the effects observed in PZT 87/13 crystal; in particular the presence of the monoclinic phases and the polarization vector rotation between these phases under electric field action. The induced shear piezoelectric coefficients, complicated domain structures, and their dynamics determine the appearance of drastic piezoelectric activity at 195 °C. We want to point out that 'unusual temperatures' may exist in a crystal where phases with different symmetries coexist. In the investigated crystal, it is the temperature of 250 °C, at which the disappearance of piezoelectric activity can be related to the state of randomly oriented and also overlapping domains of small sizes. In this case, the crystal behaves locally like an isotropic medium.

4. Conclusions

A strong piezoelectric response has been found in the recently discovered phase in PZT 87/13 above 200 °C. The piezoelectric coefficient d_{33} can reach values exceeding 2500 pm V^{-1}.

The coexistence of monoclinic and rhombohedral phases has been found by observation of optical orientation populations in a function of temperature. This complex phase coexistence makes polarization vector rotation much better manageable, making extrinsic contribution to the piezoelectric response. Another contribution to the extrinsic effect comes from the finely divided domain structures that should appear due to an increase in the number of M domains (24 types possible) at the expense of R domains (6 types possible). Such a fine structure also increases the movements of domain walls, which make yet another extrinsic contribution to the piezoelectric effect.

Due to the complex phase coexistence, and thus domain structures induced under the influence of a strong electric field, spontaneous polarization vectors may easily rotate in different directions. If spontaneous polarization directions in different overlapping small domains are random, then on the average, the crystal behaves like an isotropic one, and locally the piezoelectric effect may disappear, as has been observed in quasi-static measurements near 250 °C.

The high piezoelectric effect in PZT 87/13 single crystal under strong electric field action is connected with polarization direction changes inside domains, motions of domain walls, electrical and mechanical interactions of neighboring domains, and rotation of polarization vector. The contribution of all these factors determines the high piezoelectric response in Zr-rich PZT crystals. In the investigated single PZT 87/13 crystal, it takes primary role around 195 °C, i.e., in the vicinity of the recently discovered phase transition temperature, where instability in the octahedral tilts subsystem has been already postulated [30,31].

Declaration of Competing Interest

The authors declare no conflict of interest.

Acknowledgement

Supplementary materials

Supplementary material associated with this article can be found, in the online version, at doi:10.1016/j.actamat.2021.117129.

References

[1] W. Heywang, K. Lubitz, W. Wersing, Piezoelectricity, Springer-Verlag, Berlin Heidelberg, Germany, 2008.

[2] M.T. Chorsi, E.J. Curry, H.T. Chorsi, R. Das, J. Baroody, P.K. Purohit, H. Ilies, T.D. Nguyen, Piezoelectric Biomaterials for Sensors and Actuators, Adv. Mater. 31 (2019) 1802084.

[3] A. Marino, G.G. Genchi, V. Mattoli, G. Ciofani, Piezoelectric nanotransducers: the future of neural stimulation, Nano Today 14 (2017) 9–12.

[4] H. Sato, Y. Shimojo, T. Sekiya, Application of metal core-piezoelectric fiber – embedment in CFRP, Repair. Struct. Compos. Wraps (2003) 257–264.

[5] M. Kim, K.-.S. Yun, Helical piezoelectric energy harvester and its application to energy harvesting garments, Micromachines (Basel) 8 (2017) 115.

[6] Q. Dong, T. Ishima, H. Kawashima, W. Long, Study on the spray characteristics of a piezo- pintle type injector for DI gasoline engines, J. Mech. Sci. Tech. 27 (2013) 1981–1993.

[7] M.A. Johnson, Exploring the cantilever: teaching tools for atomic force microscopy, Eur. J. Phys. 41 (2020) 045807.

[8] M. Khalili, A.B. Bitenb, G. Vishwakarmab, S. Ahmedb, A.T. Papagiannakis, Electro-mechanical characterization of a piezoelectric energy harvester, Appl. Energy 253 (2019) 113585.

[9] T. Yoshimura, H. Miyabuchi, S. Murakami, A. Ashida, N. Fujimura, Characterization of direct piezoelectric properties for vibration energy harvesting, Mater. Sci. Eng. 18 (2011) 092026.

[10] D. Damjanovic, Contributions to the piezoelectric effect in ferroelectric single crystals and ceramics, J. Am. Ceram. Soc. 88 (2005) 2663–2676.

[11] B. Noheda, D.E. Cox, G. Shirane, S.-.E. Park, L.E. Cross, Z. Zhong, Polarization rotation via a monoclinic phase in the piezoelectric $92\%PbZn_{1/3}Nb_{2/3}O_3$-$8\%PbTiO_3$, Phys. Rev. Lett. 86 (2001) 3891–3894.

[12] D. Vanderbilt, M.H. Cohen, Monoclinic and triclinic phases in higher-order Devonshire theory, Phys. Rev. B 63 (2001) 094108.

[13] H. Fu, R.E. Cohen, Polarization rotation mechanism for ultrahigh electromechanical response in single-crystal piezoelectrics, Nature 403 (2000) 281–283.

[14] R. Guo, L.E. Cross, S.-.E. Park, B. Noheda, D.E. Cox, G. Shirane, Origin of the High Piezoelectric Response in $PbZr_{1-x}Ti_xO_3$, Phys. Rev. Lett. 84 (2000) 5423–5426.

[15] H. Choe, J. Bieker, N. Zhang, A. M.Glazer, P.A. Thomas, S. Gorfman, Monoclinic distortion, polarization rotation and piezoelectricity in the ferroelectric $Na_{0.5}Bi_{0.5}TiO_3$, IUCrJ 5 (2018) 417–427.

[16] N. Zhang, H. Yokota, A.M. Glazer, Z. Ren, D.A. Keen, D.S. Keeble, P.A. Thomas, Z.-.G. Ye, The missing boundary in the phase diagram of $PbZr_{1-x}Ti_xO_3$, Nat. Commun. 5 (2014) 5231.

[17] B. Jaffe, W.R. Cook, H. Jaffe, Piezoelectric Ceramics, Academic Press, London, UK, 1971.

[18] B. Jaffe, R.S. Roth, S. Marzullo, Piezoelectric properties of lead zirconate-lead titanate solid-solution ceramics, J. Appl. Phys. 25 (1954) 809–810.

[19] Y. Xie, PhD thesis, Simon Fraser University Burnaby Canada, 2013.

[20] R.W. Whatmore, R. Clarke, A.M. Glazer, Tricritical behaviour in $PbZr_xTi_{1-x}O_3$ solid solutions, J. Phys. C: Solid State Phys. 11 (1978) 3089–3102.

[21] I. Lazar, M. Oboz, J. Kubacki, A. Majchrowski, J. Piecha, D. Kajewski, K. Roleder, Weak ferromagnetic response in $PbZr_{1-x}Ti_xO_3$ single crystals, J. Mater. Chem. C 7 (2019) 11085–11089.

[22] R.G. Burkovsky, Y.A. Bronwald, A.V. Filimonov, A.I. Rudskoy, D. Chernyshov, A. Bosak, J. Hlinka, X. Long, Z.-.G. Ye, S.B. Vakhrushev, Structural heterogeneity and diffuse scattering in morphotropic lead zirconate-titanate single crystals, Phys. Rev. Lett. 109 (2012) 097603.

[23] D. Phelan, X. Long, Y. Xie, Z.-.G. Ye, A.M. Glazer, H. Yokota, P.A. Thomas, P.M. Gehring, Single crystal study of competing rhombohedral and monoclinic order in lead zirconate titanate, Phys. Rev. Lett. 105 (2010) 207601.

[24] S. Gorfman, D.S. Keeble, A.M. Glazer, X. Long, Y. Xie, Z.-.G. Ye, S. Collins, P.A. Thomas, High-resolution x-ray diffraction study of single crystals of lead zirconate titanate, Phys. Rev. B 84 (2011) 020102.

[25] A.A. Bokov, X. Long, Z.-.G. Ye, Optically isotropic and monoclinic ferroelectric phases in $Pb(Zr_xTi_{1-x})O_3$ (PZT) single crystals near morphotropic phase boundary, Phys. Rev. B 81 (2010) 172103.

[26] I. Lazar, S.H. Oh, J.-.H. Ko, P. Zajdel, D. Kajewski, A. Majchrowski, J. Piecha, J. Koperski, A. Soszyński, K. Roleder, Additional phase transition in a $PbZr_{0.87}Ti_{0.13}O_3$ single crystal, J. Phys. D: Appl. Phys. 52 (2019) 115302.

[27] I. Lazar, D. Kajewski, A. Majchrowski, A. Soszyński, J. Koperski, K. Roleder, A contribution to understanding the complex phase diagram of PZT compounds, Ferroelectrics 500 (2016) 67–75.

[28] J. Frantti, Y. Fujioka, A. Puretzky, Y. Xie, Z.-.G. Ye, A.M. Glazer, A statistical model approximation for perovskite solid-solutions: a Raman study of lead-zirconate-titanate single crystal, J. Appl. Phys. 113 (2013) 174104.

[29] I. Lazar, A. Majchrowski, A. Soszyński, K. Roleder, Phase Transitions and Local Polarity above T_C in a $PbZr_{0.87}Ti_{0.13}O_3$ Single Crystal, Crystals 10 (2020) 286.

[30] F. Cordero, F. Trequattrini, F. Craciun, C. Galassi, Octahedral tilting, monoclinic phase and the phase diagram of PZT, J. Phys.: Condens. Matter 23 (2011) 415901.

[31] F. Cordero, F. Trequattrini, F. Craciun, C. Galassi, Merging of the polar and tilt instability lines near the respective morphotropic phase boundaries of $PbZr_{1-x}Ti_xO_3$, Phys. Rev. B 87 (2013) 094108.

[32] B. Jaffe, R.S. Roth, S. Marzullo, Properties of piezoelectric ceramics in the solid–solution series lead titanate-lead zirconate-lead oxide-tin oxide and lead titanate-lead hafnate, J. Res. Natl. Bur. Stand (1934) 55 (1955) 239–254.

[33] A. Bauer, D. Buhling, H.J. Gesemann, G. Helke, W. Schreckenbach, Technology and application of ferroelectrics, Akademische Verlagsgesellschaft Geest & Portig K.-G, Leipzig, Germany 1976.

[34] K. Roleder, I. Franke, A.M. Glazer, P.A. Thomas, S. Miga, J. Suchanicz, The piezoelectric effect in $Na_{0.5}Bi_{0.5}TiO_3$ ceramics, J. Phys.: Condens. Matter 14 (2002) 5399–5406.

[35] K. Roleder, Measurement of the high-temperature electrostrictive properties of ferrpelectrics, J. Phys. E: Scientific Instrum. 16 (1983) 1157–1159.

[36] M.A. Geday, J. Kreisel, A.M. Glazer, K. Roleder, Birefringence imaging of phase transitions: application to $Na_{0.5}Bi_{0.5}TiO_3$, J. Appl. Crystal. 33 (2000) 909–914.

[37] M.A. Geday, W. Kaminsky, J.G. Lewis, A.M. Glazer, Images of absolute retardance L•Δn, using the rotating polariser method, J. Microscopy 198 (2000) 1–9.

[38] N. Zhang, H. Yokota, A.M. Glazer, D.A. Keen, S. Gorfman, P.A. Thomas, W. Ren, Z.-.G. Ye, Local-scale structures across the morphotropic phase boundary in $PbZr_{1-x}Ti_xO_3$, IUCrJ 5 (2018) 73–81.

[39] Z. Wang, N. Zhang, H. Yokota, A.M. Glazer, Y. Yoneda, W. Ren, Z.-.G. Ye, Local structures and temperature-driven polarization rotation in Zr-rich $PbZr_{1-x}Ti_xO_3$, Appl. Phys. Lett. 113 (2018) 012901.

[40] A.M. Glazer, P.A. Thomas, K.Z. Baba-Kishi, G.K.H. Pang, C.W. Tai, Influence of short-range and long-range order on the evolution of the morphotropic phase boundary in $PbZr_{1-x}Ti_xO_3$, Phys. Rev. B 70 (2004) 184123.

[41] R. Zhang, B. Jiang, W. Cao, Elastic, piezoelectric, and dielectric properties of multidomain $0.67PbMg_{1/3}Nb_{2/3}O_3$–$0.33PbTiO_3$ single crystals, J. Appl. Phys. 90 (2001) 3471–3475.

[42] S. Wada, K. Yako, H. Kakemoto, T. Tsurumi, Enhanced piezoelectric properties of barium titanate single crystals with different engineered-domain sizes, J. Appl. Phys. 98 (2005) 014109.

[43] S. Gorfman, H. Choe, G. Zhang, N. Zhang, H. Yokota, A.M. Glazer, Y. Xie, V. Dyadkin, D. Chernyshov, Z.-.G. Ye, New method to measure domain-wall motion contribution to piezoelectricity: the case of $PbZr_{0.65}Ti_{0.35}O_3$ ferroelectric, J. Appl. Cryst. 53 (2020) 1039–1050.

[44] A.J. Bell, P.M. Shepley, Y. Li, Domain wall contributions to piezoelectricity in relaxor-lead titanate single crystals, Acta Mater. 195 (2020) 292–303.

[45] S. Gorfman, A.M. Glazer, Y. Noguchi, M. Miyayama, H. Luo, P.A. Thomas, Observation of a low-symmetry phase in $Na_{0.5}Bi_{0.5}TiO_3$ crystals by optical birefringence Microscopy, J. Appl. Cryst. 45 (2012) 444–452.

[46] J. Erhart, Domain wall orientations in ferroelastics and ferroelectrics, Phase Transitions 77 (2004) 989–1074.

[47] N. Zhang, S. Gorfman, H. Choe, T. Vergentev, V. Dyadkin, H. Yokota, D. Chernyshov, B. Wang, A.M. Glazer, W. Rena, Z.-.G. Ye, Probing the intrinsic and extrinsic origins of piezoelectricity in lead zirconate titanate single crystals, J. Appl. Cryst. 51 (2018) 1396–1403.

[48] L. Bellaiche, A. Garcia, D. Vanderbilt, Electric-field induced polarization paths in $PbZr_{1-x}Ti_xO_3$ alloys, Phys. Rev. B 64 (2001) 060103.

[49] J.F. Nye, Physical Properties of Crystals Their Representation by Tensors and Matrices, Clarendon Press, Oxford, UK, 1985.

[50] T. Sluka, A.K. Tagantsev, D. Damjanovic, M. Gureev, N. Setter, Enhanced electromechanical response of ferroelectrics due to charged domain walls, Nat. Commun. 3 (2012) 748.

[51] S.E. Park, T.R. Shrout, Characteristics of relaxor-based piezoelectric single crystals for ultrasonic transducers, IEEE Trans. Ultrason. Ferroelectr. Freq. Control 44 (1997) 1140–1147.

[52] S. Wada, S.E. Park, L.E. Cross, T.R. Shrout, Engineered domain configuration in rhombohedral PZN-PT single crystals and their ferroelectric related properties, Ferroelectrics 221 (1999) 147–155.

[53] D. Damjanovic, F. Brem, N. Setter, Crystal orientation dependence of the piezoelectric d_{33} coefficient in tetragonal $BaTiO_3$ as a function of temperature, Appl. Phys. Lett. 80 (2002) 652–654.